REALIZATION OF POWER DISTRIBUTION IN BETWEEN ENERGY GENERATION AND STORAGE SYSTEM IN MICROGRID BY USING IBDC WITH EPS CONTROL

G.Suresh

G.Suresh,Lecturer in EEE,Govt. Polytechnic, Anantapur.

ABSTRACT: Now a days the energy demand of power supply is keep on increasing. But we are unable to meet the concerned demand of power supply. These are mainly due to we are getting more amount of energy from Conventional Energy sources like Thermal power stations, Hydro electric power stations and Nuclear power stations. Among them thermal power stations under low efficiency. Fortunately, some countries like India more depending the Thermal power stations. Which are not economical and eco-friendly. Due to the above factors it required to concentrate on the Non-Conventional Energy sources like Wind, Solar, Geo thermal, Tidal e.t.c There is lot of drawbacks in the utilization of Non-conventional energy sources. Among them, frequency matching, unit commitment and DC power generation are major problems. We know that most of non conventional energy sources like solar, geothermal can able to generate the power in the form power of DC only. But it is required to transmit the power in the form AC only. By using some we can come across these problems. We know that the frequency matching and the unit commitment are very important factors in the transmission AC power. In order to utilize the Non-Conventional Energy sources, at present a method is named as Traditional Phase Shift control technique is used in order to avoid the problems arised in utilization of Non-Conventional Energy sources such as frequency matching, unit commitment. This is a effective method in order avoid these problems. But because this method it poses some more disadvantages apart from the frequency matching, unit commitment which are undesirable. They are is as follows high current stress, high back flow power, high conductional losses, high circulating currents, limited regulating range of transmission, high switching losses, low regulating flexibility and low efficiency. These are all drawbacks in the present Traditional Phase Shift control system. The problems which were arised in the Traditional Phase Shift Control can be overcome by a new method which is named as Extended Phase Shift control technique. This was obtained by changing the control scheme in an extended manner. The proposed method, Extended Phase Shift control overcome whatever the disadvantages occurred in the Traditional Phase Shift control, as like as high current stress, high back flow power, high conductional losses, high circulating currents, limited regulating range of transmission, high switching losses, low regulating flexibility and low efficiency. It means that Traditional Phase shift control just overcome the problems whatever occur in the utilization Non-Conventional Energy sources, but by using this method we are unable to utilize the concerned energy sources in effective manner. Whereas by using the new method Extended Phase Shift control we can utilize the Non-Conventional energy sources effectively, this is desired one. This entire project should provide entire information regarding various controlling methods. It is concentrate more on the Extended Phase Shift control. The entire analysis of Extended phase shift control, various control methods will be analyzed by using MATLAB/SIMULINK. By using this software we got relevant waveforms to analyze.

1. INTRODUCTION

1.1 Fuel Cells

1.1.1 Introduction

Fuel cells convert fuel and air directly to electricity, heat and water in an electrochemical process. Unlike conventional engines, they do not burn the fuel and run pistons or shafts, and so have fewer efficiency losses, low emissions and no moving parts.

In principle a fuel cell operates like a battery. However, unlike a battery, it will not run down while it continues to be supplied with fuel and air. It is an essentially clean technology that uses hydrogen (from its fuel source) and oxygen (from the air) to generate electricity and heat without combustion or pollution, its only basic emission being vaporized water.

1.1.2 Basic Principle of operation a Fuel Cell

In the fuel cell hydrogen and oxygen react to create water, electricity and heat, which can be used in various applications. The reaction is essentially the reverse of electrolysis. There is no noise or mechanical movement involved. The fuel cell is like a battery, the only difference being that as long as hydrogen is provided it will continue to provide power.

Hydrogen (1) and oxygen is supplied on each side of a cell. The cell consists of an electrolyte membrane with a catalyst layer on each side. When hydrogen is lead to the first catalyst layer, the anode, the hydrogen molecules are split into their basic elements, a proton (2) and an electron. The protons migrate through the electrolyte membrane (4) to the second catalyst layer, the cathode. Here they react with oxygen to form water (5). At the same time the electrons are

forced to travel around the membrane to the cathode side, because they cannot pass the membrane. This movement of electrons thus creates an electrical current (3).

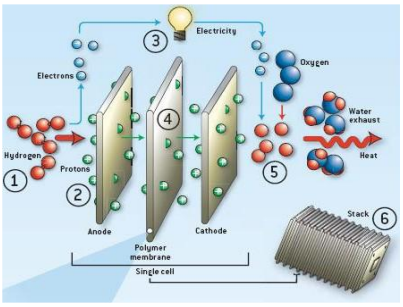

Fig. 1.1: Fuel cell chemistry

Here they react with oxygen to form water (5). At the same time the electrons are forced to travel around the membrane to the cathode side, because they cannot pass the membrane. This movement of electrons thus creates an electrical current (3).

A typical fuel cell produces 0.5-1 volt. The appropriate voltage level for a specific application is achieved by combining a number of single cells in series and parallel circuits to form a fuel cell stack.

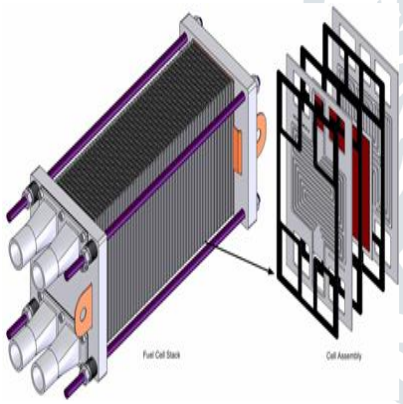

Fig. 1.2: A fuel cell stack

1.2 Ultra capacitors

1.2.1 Introduction

Like batteries, ultracapacitors are energy storage devices. They use electrolytes and configure various-sized cells into modules to meet the power, energy, and voltage requirements for a wide range of applications. But batteries store charges chemically, whereas ultracapacitors store them electrostatically.

1.2.2 Principle of Operation

Ultracapacitors are true capacitors in that energy is stored via charge separation at the electrode electrolyte interface, and they can withstand hundreds of thousands of charge/discharge cycles without degrading. An ultracapacitor, also known as a double-layer capacitor, polarizes an electrolytic solution to store energy electrostatically. Though it is an electrochemical device, no chemical reactions are involved in its energy storage mechanism. This mechanism is highly reversible, and allows the ultracapacitor to be charged and discharged hundreds of thousands of times.

An ultracapacitor can be viewed as two nonreactive porous plates, or collectors, suspended within an electrolyte, with a voltage potential applied across the collectors. In an individual ultracapacitor cell, the applied potential on the positive electrode attracts the negative ions in the electrolyte, while the potential on the negative electrode attracts the positive ions. A dielectric separator between the two electrodes prevents the charge from moving between the two electrodes.

Once an ultracapacitor is charged and energy stored, a load can use this energy. The amount of energy stored is very large compared to a standard capacitor because of the enormous surface area created by the porous carbon electrodes and the small charge separation created by the dielectric separator. However, it stores a much smaller amount of energy than does a battery. Since the rates of charge and discharge are determined solely by its physical properties, the ultracapacitor can release energy much faster (with more power) than a battery that relies on slow chemical reactions.

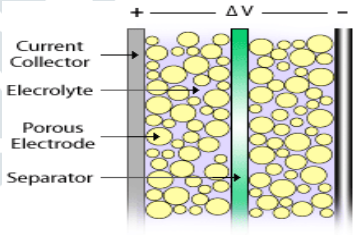

Figure 1.3: Individual ultracapacitor cell

A single ultracapacitor can only produce a potential of 2,5-2,7 voltage. For moste applications this it not enough, so the ultracapacitors has to be aligned in a konstellation of serial and parallel connections, to obtain the desired voltage and energy. Further more to utilize the ultracapacitor effectively it is not desired to discharge them more than to half the rated voltage. In this way it is possible to obtain 75% of the initial stored energy.

1.3 UPS Load

A UPS(Uninteruptible Power System - UPS) is a emergency power generating unit. It takes over the supply of electrical power for a critical load at a power outage. The critical load will hereby function undisturbed. The UPS works with a voltage range of pm160 − 220V , but it has been decided on a voltage output of ±200V , from the DC-DC converter.

1.4 Microgrid

Microgrids are becoming a reality in a scenario in which interconnected loads, distributed energy resources, and distributed storage systems can be conjugated and integrated into grid. The need for more flexible electricity systems, energy savings, and environmental impact are driving the development of microgrids [2]–[6].

Generally, microgrids can operate in grid-connected mode and islanded mode [7], [8]. In the grid-connected mode, the microgrid is connected to a utility grid, operates in parallel with the utility, and exchanges power with the utility through the point of common coupling. However, microgrid disconnects the utility and transfers into the islanded operation when a fault occurs in the upstream power grid. And in the islanded mode, microgrid can work as an autonomous grid to generate electricity using distributed energy resources. So it is important to balance demand and supply coming both from the utility and distributed energy resources. Moreover, due to not only environmental aspects but also social, economical, and political interests, many types of renewable energy, such as photovoltaic (PV) and wind energy, have been widely utilized as distributed energy resources in microgrid [6].

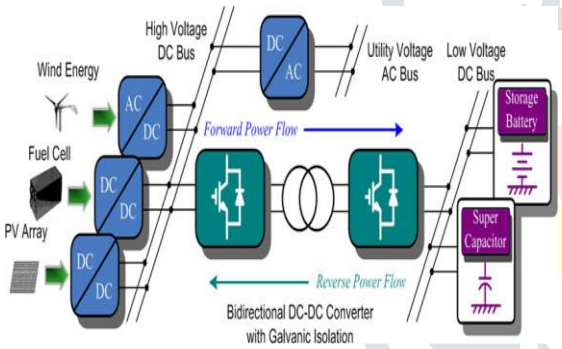

Fig. 1.4. Typical application of BDC for power distribution in microgrid [12].

Generally, BDC is divided into non isolated type [13], [14] and isolated type [12], [15], and galvanic isolation for BDC is required for flexibility of system reconfiguration and meeting safety standards [15].

1.6 Isolated Bi-Directional DC-DC Converter

State-of-the-art isolated bidirectional DC–DC converter (IBDC) is based on the single-phase and H-bridge topology with a high-frequency isolation transformer. Fig. 1.2 depicts a typical configuration of IBDC.

Bi-Directional DC-DC Converters + Isolation Transformer = IBDC

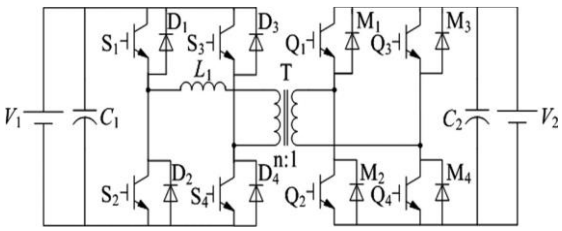

Fig. 1.5. Typical configuration of IBDC.

1.5 Bi-Directional DC-DC Converters

The variable nature of these renewable energy systems relies on natural phenomenon, such as sunshine or wind [9], [10]. Consequently, it is difficult to predict the power that can be obtained through these prime sources, and the peaks of power demand do not coincide necessarily with the generation peaks. Hence, storage energy systems are required if we want to supply the local loads in an uninterruptible power supply (UPS) fashion [6], [11].

In order to realize power distribution between energy generation systems and storage systems in micro grids, various bi-directional DC–DC converters (BDCs) have been proposed as an everlasting key component to interface between a high-voltage bus, where an energy generation system such as a fuel cell stack or a photovoltaic array is installed, and a low-voltage bus, where usually an energy storage system such as a battery or a super capacitor is implemented, as shown in Fig. 1.4 [12].

1.7 Traditional Pulse Width Modulation

1.7.1 Introduction

Generally, there are mainly two kinds of control methods for such topology traditional pulse width modulation (PWM) control and phase-shift control.

1.7.2 Basic Principle of Operation

In traditional PWM control, the cross-connected switch pairs in H-bridge (H1)(Shown in figure 1.2, such as(S1 ,S4) and (S2 ,S3) , are switched in turn to transform the high voltage V1 from DC to AC, the switches (Q1 –Q4) in H-bridge (H2) are turned OFF and the current conducts only through the diodes (M1 –M4) to transform the voltage from AC to DC, so the power is transferred from V1 side to V2 side. In the reverse power flow, the states of S1 –S4 and Q1 –Q4 are exchanged. This control method is simple and easy to implement, but it has poor dynamic performance. And the AC output voltage can only be lower than DC input voltage in H-bridge inverter, so its regulating range of voltage is limited.

2. ADVANCED CONTROL TECHNIQUES OF IBDC

2.1 TRADITIONAL PHASE SHIFT (TPS) CONTROL

2.1.1 Introduction

Traditional Pulse Width Modulation control method is simple and easy to implement, but it has poor dynamic performance. And the AC output voltage can only be lower

than DC input voltage in H-bridge inverter, so its regulating range of voltage is limited. Because these factors like limitation of regulating range of voltage and poor dynamic performance the Traditional Phase Shift Control is preferred even though design control scheme is difficult as compared to Traditional Pulse Width Modulation Control.

2.2 Basic Principle of Operation

In TPS control [15], [16], the cross-connected switch pairs in both H-bridges (H1 and H2) are switched in turn to generate phase-shifted transition square waves to the transformer's primary and secondary sides. And the corresponding phase shift changes the voltage across the transformer's leakage inductor to manipulate the power flow direction and magnitude. This control method is attracting more and more attention due to its advantages such as small inertia, high dynamic performance, easy to realize soft-switching control, and so on.

But in this method, the control of the power flow is dependent on transformer's leakage inductor that result in great circulating power and current stress when the value of V1 /nV2 deviate far from 1, where n is turns' ratio of the transformer. And then, the loss in power devices and magnetic components is increased and the efficiency of converter is reduced. In order to improve the performance of the IBDC, various control methods were explored [18].

In some of these studies, the duty ratio of the driving signals of each semiconductor device is variable, and should be calculated online, that increases the complexity of the control. Some studies are focused on how to extend the soft-switching range or eliminate reactive power [17], the detailed analysis of steady characteristics is not conducted. In [18], a novel phase-shift dual-half-bridge converter with an adaptive inductor was proposed. It utilizes an adaptive inductor as the commutation inductor to adapt to the change of the output power, which results in strict requirements of the coiling method of inductor and the complexity of the control. And it is mainly improvement of hardware design; the control method of the proposed converter is still TPS control.

In view of the study situation mentioned above, this project points out a phenomenon of power backflow in traditional phase shift control, and analyzes the effects which backflow power act on power circulating flow and current stress. On this basis, the paper presents a novel extended-phase-shift control of IBDC for power distribution in microgrid. Different from the control methods mentioned above, this method adds another degree of freedom to the converter by adjusting the time sequence between the driving signals of diagonal semiconductor switches, e.g., (S1 ,S4) in Fig. 1.5. It not only has smaller power circulating flow and current stress, but also expands regulating range of transmission power and enhances regulating flexibility.

2.3 Phenomenon of Power Backflow

We replace the transformer with T-type equivalent circuit (In Fig. 1.5,), and considering that the magnetizing inductance of the transformer is much greater than its leakage inductance, the magnetizing inductance can be considered as an open circuit. Therefore, the converter in phase-shift control can be represented by a simplified scheme comprised of two square waves' voltage sources linked by an inductance L, as shown in Fig. 2.1.

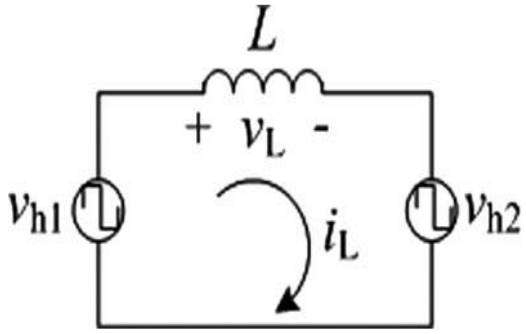

Fig. 2.1. Equivalent circuit of phase-shift control.

In Fig. 2.1, L is the sum of the transformer leakage inductance and that of the auxiliary inductor L_1 , v_{h1} and v_{h2} are the equivalent AC output voltages of H1 and H2 in V_1 side, respectively, v_L and i_L are the voltage and current of inductor L, respectively. The power-flow direction and magnitude can simply be controlled by adjusting the phase shift between v_{h1} and v_{h2} .Here we take the forward power flow (from V_1 to V_2) as an example to analyze the main operation principle of TPS control.

The main waveforms of IBDC in TPS control are shown in Fig. 2.2, where pin is the transient waveform of transmission power, T_{hs} is a half switching period, and D is the phase-shift ratio between the primary and secondary voltages of the isolation transformer, where $0 \leq D \leq 1$.Andweassume $V_1 \geq nV_2$ in Fig. 2.2, the other condition $V_1 < nV_2$ can be analyzed similarly. Because v_{h1} and v_{h2} are both square wave AC voltages and their interaction is through the inductor L, so the phase of the primary current is not always the same as the primary voltage.

As can be seen from Fig. 2.2, i_L is of the opposite phase from v_{h1} for an interval of $t = t_0 \sim t'_0$ and $t = t_2 \sim t'_2$, that is a portion of the power delivered to the V_2 side in one switching period, while the other portion is sent back to the primary voltage source V_1 . We defined it as backflow power, which is the dark-shaded area in Fig. 2.2. For a given transmission power, with the increase of the backflow power, the forward power also increases to compensate the loss caused by backflow power. Then the circulating power and current stress are increased, which result in great loss in power devices and magnetic components and low efficiency of converter.

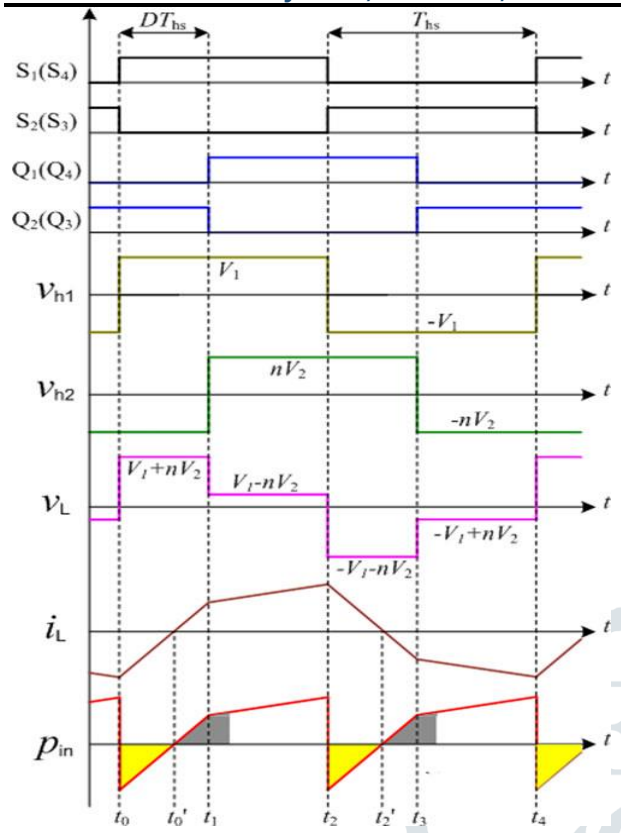

Fig. 2.2. Waveforms of IBDC in TPS control.

2.4 EXTENDED PHASE SHIFT (EPS) CONTROL

2.4.1 Introduction

The Traditional Phase shift control is more advantageous than Traditional Pulse Width Modulation control especially in the parameters like dynamic performance and regulating range of voltage.

But in this method, the control of the power flow is dependent on transformer's leakage inductor that result in great circulating power and current stress when the value of V_1 / nV_2 deviate far from 1, where n is turns' ratio of the transformer. And then, the loss in power devices and magnetic components is increased and the efficiency of converter is reduced. In order to improve the performance of the IBDC, various control methods were explored [18]. In some of these studies, the duty ratio of the driving signals of each semiconductor device is variable, and should be calculated online, that increases the complexity of the control. Some studies are focused on how to extend the soft-switching range or eliminate reactive power [17], the detailed analysis of steady characteristics is not conducted.

Among the some control methods The Extended Phase Shift Control is Preferred it is because of its own advantages over the exited Traditional Phase Shift Control these will be discussed in this project.

2.5 Basic Principle of Operation

In order to significantly decrease the backflow power of the converter, vh1 should not be confined to square waveforms with 50% duty ratio. For example, if S1 and S4 do not have the same driving signal but has a phase-shift ratio of D_1, as shown in Fig. 3.1, the transformer primary voltage will emerge as a three level instead of the traditional two-level. Then the behaviours of i_L will also be changed: the backflow appearance time ($t = t_0 \sim t'_0$ and $t = t_2 \sim t'_2$) in Fig. 3.1 are divided into two intervals ($t = t_0 \sim t'_1$, $t = t_1 \sim t'_1$ and $t = t_3 \sim t'_4$, $t = t_4 \sim t'_4$) in Fig.3.1 respectively. And the transformer primary voltage $v_{h1} = 0$, i.e., backflow power is 0, when $t = t_0 \sim t'_1$ and $t = t_3 \sim t'_4$.So the backflow power is decreased for a given transmission power. In the reverse power flow, we just need to exchange the operating states of the H-bridges H_1 and H_2.

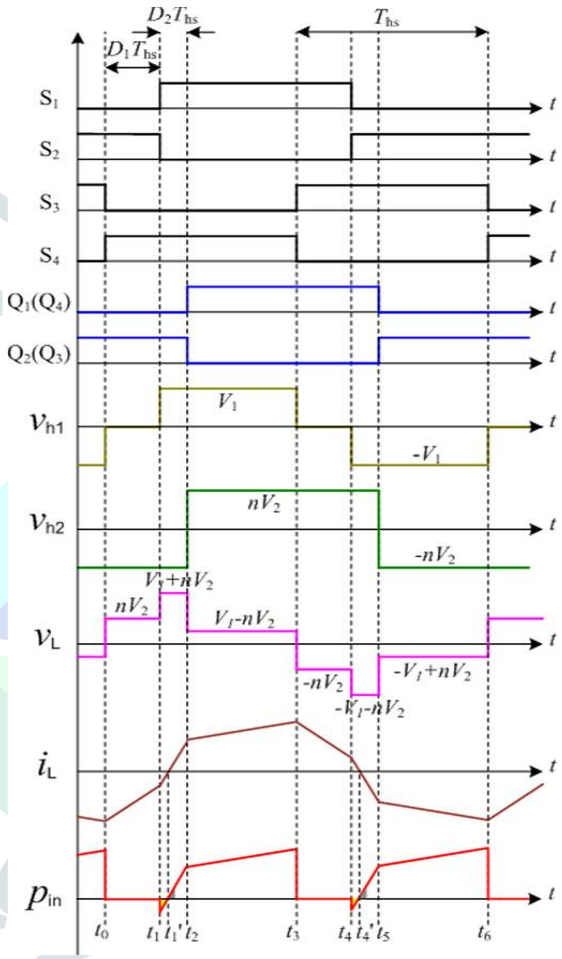

Fig. 2.3. Waveforms of IBDC in EPS control.

In Fig. 2.3, D_1 is the phase-shift ratio between the driving signals of S_1 and S_4 or S_2 and S_3 in H-bridge H_1 , we defined its inner phase-shift ratio, where $0 \le D_1 \le 1$. D_2 is the phase-shift ratio between the primary and secondary voltages of the isolation transformer, we defined its outer phase-shift ratio, where $0 \le D_2 \le 1$ and $0 \le D_1+D_2 \le 1$. In fact, compared to the TPS control, there is not only the outer phase-shift ratio but also the inner phase-shift ratio in the proposed EPS control, which will decrease the current stress, expands regulating range of transmission power and enhances regulating flexibility.

To simplify the process of the analysis, we assume that the converter has reached steady operation states. From Fig. 3.1, the switching cycle can be divided into eight operation modes which are explained as follows

2.6 Operation Modes of IBDC in Extended-Phase-Shift Control

2.6.1 Mode 1

Duration of this mode is for t_0 -- t'_1 Fig. 2.4 shows the equivalent circuit for the mode 1. Just before t_0 ,S_2 and S_3 are conducting. The current i_L is in negative direction. At t_0 ,S_3 is turned OFF and S_4 is turned ON at zero current, and D_4 starts to conduct. On the secondary side, the current is carried from L to V_2 by M_2 and M_3 .The voltage across L is clamped at nV_2 , and the current i_L decreases linearly. This mode ends up when S_2 is turned OFF. During this mode, the current of L is

$$i_L(t) = i_{L0}(t_0) + \frac{nV_2}{L}(t - t_0) \quad \text{.... (3.1)}$$

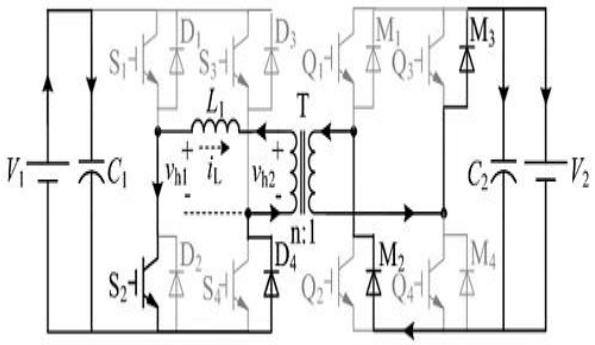

Fig 2.4 Equivalent Circuit Diagram of IBDC in Mode-1 Operation

2.6.2 Mode 2

Duration of this mode is for t_1 -- t'_1. Fig. 2.5 shows the equivalent circuit for mode 2. If current i_L is still in negative direction at t_1 then at t_1, S_2 is turned OFF and S_1 is turned ON at zero current, i_L is carried from L to V_1 by D_1 and D_4. On the secondary side, the current is carried from L to V_2 by M_2 and M_3. The voltage across L is clamped at V_1+nV_2 , and i_L still decreases linearly. This mode ends up with i_L decreasing to zero. During this mode, i_L is

$$i_L(t) = i_L(t_1) + \frac{V_1+nV_2}{L}(t - t_1)$$

... (3.2)

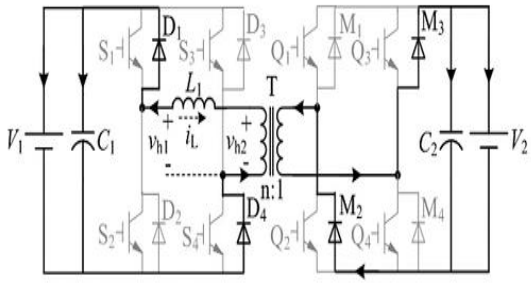

Fig 2.5 Equivalent Circuit Diagram of IBDC in Mode-2 Operation

2.6.3 Mode 3

Duration of this mode is for t'_1-- t_2. Fig. 2.6 shows the equivalent circuit for the mode 3. At t'_1 , the polarity of i_L changes from negative to positive. And because the driving signals of S_1 ,S_4 ,Q_2 , and Q_3 are already on, so S_1 ,S_4 ,Q_2 , and Q_3 start to conduct. The voltage across L is clamped at $V_1 + nV_2$, and i_L increases linearly. This mode ends up when Q_2 and Q_3 are turned OFF. During this mode, i_L is the same with 3.2

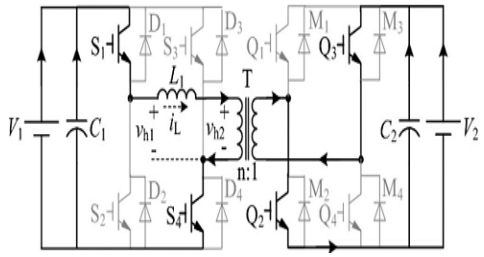

Fig 2.6 Equivalent Circuit Diagram of IBDC in Mode-3 Operation

2.6.4 Mode 4

Duration of this mode is for t_2—t_3. Fig. 2.7 shows the equivalent circuit for the mode 4.At t_2 ,Q_2 and Q_3 are turned off and Q_1 and Q_4 are turned on at zero current. M_1 and M_4 start to conduct. The voltage across L is clamped at V_1–nV_2, and i_L still increases linearly due to $V_1 \geq nV_2$. This mode ends up when S4 is turned OFF. During this mode, i_L is

$$i_L(t) = i_L(t_2) + \frac{V_1-nV_2}{L}(t - t_2) \quad \text{... (3.3)}$$

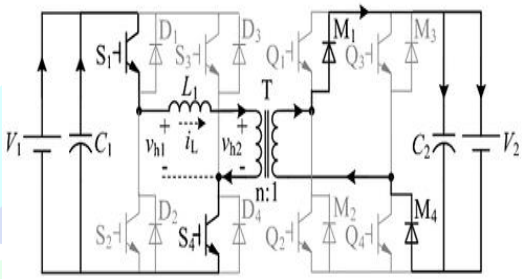

Fig 2.7 Equivalent Circuit Diagram of IBDC in Mode-4 Operation

2.6.5 Mode 5

Duration of this mode is for t_3—t_4. Fig. 2.8 shows the equivalent circuit for mode 5.At t_3 ,S_4 is turned OFF and S_3 is turned ON at zero current, D_3 starts to conduct. On the secondary side, the current is carried from L to V_2 by M_1 and M_4. The voltage across L is clamped at $-nV_2$, and the current i_L decreases linearly. This mode ends up when S_1 is turned OFF. During this mode, the current of L is

$$i_L(t) = i_L(t_3) + \frac{V_1-nV_2}{L}(t - t_3) \quad \text{... (3.4)}$$

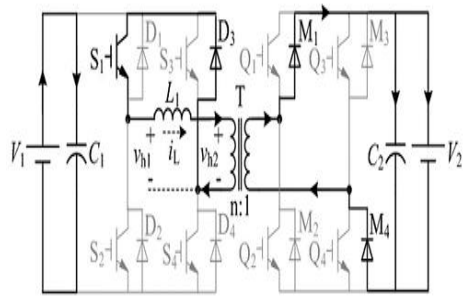

Fig 2.8 Equivalent Circuit Diagram of IBDC in Mode-5 Operation

2.6.6 Mode 6

Duration of this mode is for t_4 — t'_4. Fig. 2.9 shows the equivalent circuit for mode 6. If current i_L is still in

positive direction at t_4 , then at t_4 ,S_2 is turned OFF and S_1 is turned ON at zero current, i_L is carried from L to V_1 by D_2 and D_3 . On the secondary side, the current is carried from L to V_2 by M_1 and M_4. The voltage across L is clamped at –V1–nV2 , and i_L still decreases linearly. This mode ends up with i_L decreasing to zero. During this mode, i_L is

$$i_L(t) = i_L(t_4) + \frac{-V_1 - nV_2}{L}(t - t_4)$$

... (3.5)

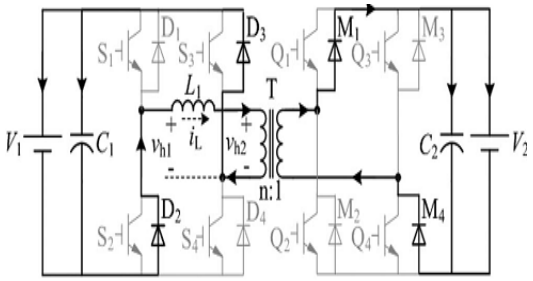

Fig 2.9 Equivalent Circuit Diagram of IBDC in Mode-6 Operation

2.6.7 Mode 7

Duration of this mode is for t'_4 — t_5. Fig. 2.10 shows the equivalent circuit for the mode 7.At t'_4 , the polarity of i_L changes from positive to negative. And, because the driving signals of S_2 ,S_3 ,Q_1 , and Q_4 are already ON, so S_2 ,S_3 ,Q_1 , and Q_4 start to conduct. The voltage across L is clamped at $–V_1–nV_2$, and i_L increases linearly. This mode ends up when Q1 and Q4 are turned OFF. During this mode, i_L is the same with Eqn. 3.5.

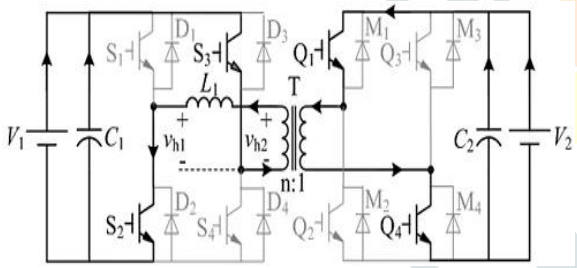

Fig 2.10 Equivalent Circuit Diagram of IBDC in Mode-7 Operation

2.6.8 Mode 8

Duration of this mode is for t_5 — t_6. Fig. 2.11 shows the equivalent circuit for the mode 8.At t_5 ,Q_1 and Q_4 are turned OFF and Q_2 and Q_3 are turned ON at zero current. M_2 and M_3 start to conduct. The voltage across L is clamped at $–V_1+nV_2$, and i_L still increases linearly due to $V_1 \geq nV_2$. This mode ends up when S3 is turned OFF. During this mode, i_L is

$$i_L(t) = i_L(t_5) + \frac{-V_1 + nV_2}{L}(t - t_5)$$

... (3.6)

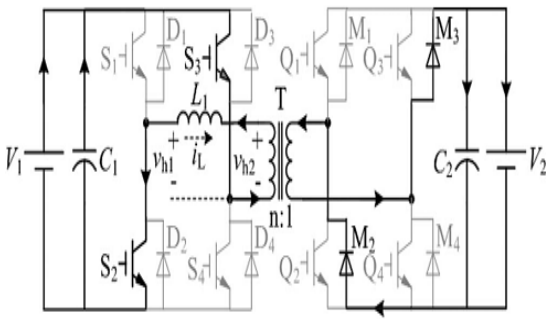

Fig 2.11 Equivalent Circuit Diagram of IBDC in Mode-8 Operation

According to the above analysis, the transformer primary voltage $v_{h1} = 0$, and there is no backflow power in modes 1 and 5. So the whole backflow power is decreased for a given transmission power. In fact, if i_L has dropped to zero before t_1 or t_4, then the backflow power will be eliminated, as shown in Fig 3.1 In this case, modes 2 and 6 in Fig. 3.3 and 3.7 will be replaced by mode 2' and 6' respectively.

2.6.9 Mode 2'

Duration of this mode is for t'_1 — t_1. Fig. 3.10 shows the equivalent circuit for mode 2'. At t'_1 , the polarity of i_L changes from negative to positive. And because the driving signals of S_2, S_4, Q_2, and Q_3 are already ON, so D_2, S_4, Q_2 and Q_3 start to conduct. The voltage across L is clamped at nV_2 , and i_L still increases linearly. This mode ends up when S_2 is turned OFF. During this mode, i_L is the same with Eqn 3.1

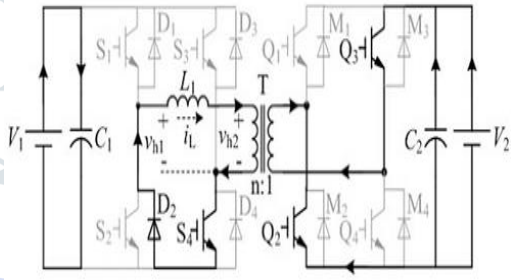

Fig 2.12 Equivalent Circuit Diagram of IBDC in Mode-2' Operation

2.6.10 Mode 6'

Duration of this mode is for t'_4 — t_4. Fig. 3.11 shows the equivalent circuit for mode 6' .At t'_4, the polarity of i_L changes from positive to negative. And because the driving signals of S_1, S_3, Q_1, and Q_4 are already ON, so D_1, S_3, Q_1, and Q_4 start to conduct. The voltage across L is clamped at $–nV_2$, and i_L still increases linearly. This mode ends up when S_1 is turned OFF. During this mode, i_L is the same with Eqn. (3.4)

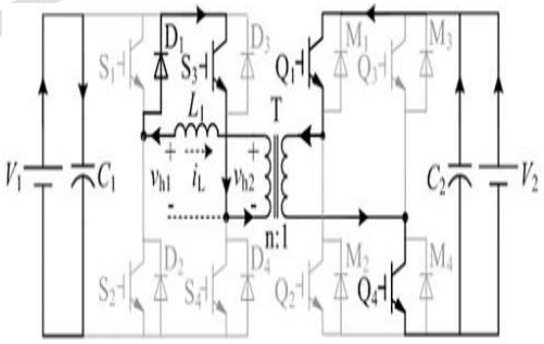

Fig 2.13 Equivalent Circuit Diagram of IBDC in Mode-6' Operation

3. ANALYSIS AND COMPARISONS OF TPS AND EPS CONTROL

3.1 Low-Frequency Average Model

According to the above analysis, assuming $t_0 = 0$, then we have $t_1 = D_1T_{hs}$, $t_2 = D_2T_{hs}$, $t_3 = T_{hs}$, $t_4 = T_{hs}+D_1$

T_{hs} , $t_5 = T_{hs}+D_2 T_{hs}$, and $t_6 = 2T_{hs}$. The average current of the inductors over one switching period ($2T_{hs}$) should be zero in steady state; thus from Eqn. (3.1) to Eqn. (3.6), we can derive

$$(t_0) = -\frac{nV_2}{4f_sL}[k(1-D_1)+(2D_1+2D_2-1)] \text{ .. (3.1)}$$

$$i_L(t_1) = -\frac{nV_2}{4f_sL}[k(1-D_1)+(2D_2-1)] \quad \text{... (3.2)}$$

$$i_L(t_2) = \frac{nV_2}{4f_sL}[k(2D_2+D_1-1)+1] \quad \text{... (3.3)}$$

Where $f_s = 1/(2T_{hs})$ is switching frequency, $k = V_1/nV_2$ is the voltage conversion ratio, and we assume $k \geq 1$ in the paper, the other condition $k < 1$ can be analyzed similarity. When the power flows from V_1 to V_2 , the current stress of converter under EPS control is

$$i'_{max} = |i_L(t_0)| = -\frac{nV_2}{4f_sL}[k(1-D_1)+(2D_1+2D_2-1)]$$

... (3.4)

The transmission power is

$$P' = \frac{1}{T_{hs}}\int_0^{T_{hs}} v_{h1}i_L(t)dt$$

$$= \frac{nV_1V_2}{2f_sL}[D_2(1-D_2)+\frac{1}{2}D_1(1-D_1-2D_2)]$$

... (3.5)

The back flow power is

$$P'_{bf} = \frac{1}{T_{hs}}\int_{t_1}^{t'_1} v_{h1}|i_L(t)|dt$$

$$= \frac{nV_1V_2[k(1-D_1)+(2D_2-1)]^2}{16Lf_s(k+1)} \quad \text{...}$$

(3.6)

where $i_L(t_1) < 0$, from Eqn. (4.2)., we have

$$k > \frac{1-2D_2}{1-D_1}$$

... (3.7)

When $k \leq (1-2D_2)/(1-D_1)$, the backflow power is zero. In Eqn. (3.1) – Eqn. (3.7), the constraints are $k \geq 1$, $0 \leq D_1 \leq 1$,$0 \leq D_2 \leq 1$, and $0 \leq D_1+D_2 \leq 1$. Similarly, from Fig. 4, the current stress of converter under TPS control is

$$i_{max} = \frac{nV_2}{4f_sL}(2D-1+k) \quad \text{... (3.8)}$$

The transmission power is

$$P = \frac{nV_1V_2}{2f_sL}D(1-D) \quad \text{... (3.9)}$$

The backflow power is

$$P_{bf} = \frac{nV_1V_2[k+(2D-1)]^2}{16f_sL(k+1)} \quad \text{... (3.10)}$$

In Eqn. (3.8) – Eqn. (3.10), the constraints are $k \geq 1$ and $0 \leq D \leq 1$. Theoretically, when the load is set as resistance R, from Eqn. (3.5), we can derive

$$V_2 = \frac{nV_1R}{2f_sL}[D_2(1-D_2)+\frac{1}{2}D_1(1-D_1-2D_2)]$$

... (3.11)

With the variation of D_1 and D_2, we have

$$0 \leq V_2 \leq \frac{nV_1R}{8f_sL} \quad \text{..(3.12)}$$

Similarly, from Eqn. 3.8, the output voltage range in the TPS control can be achieved. In fact, the output voltage range in the EPS control is the same as that in the TPS control. And its main benefit lies in that the power circulating flow and current stress are both reduced for a given output power; therefore, it leads to the improvement of the converter's overall efficiency. Theory and experiment analysis of the paper are centering on these special characteristics of EPS control as well.

3.2 Comparative Analysis of Transmission Power

For the convenience of analysis, the unified transmission power p' and p are defined as

$$\begin{cases} p' = \frac{P'}{P_N} = 4D_2(1-D_2)+2D_1(1-D_1-2D_2) \\ p = \frac{P}{P_N} = 4D(1-D) \end{cases}$$

... (3.13)

Where

$$P_N = \frac{nV_1V_2}{8f_sL}$$

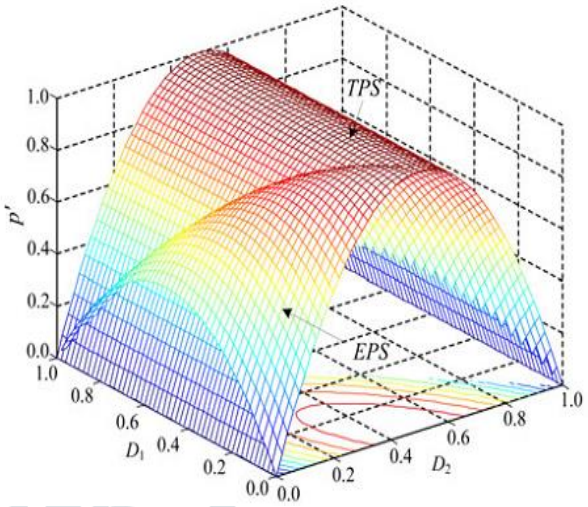

Fig. 3.1. Relation curves of the unified transmission power p' with D_1 and D_2. (3-D curves.)

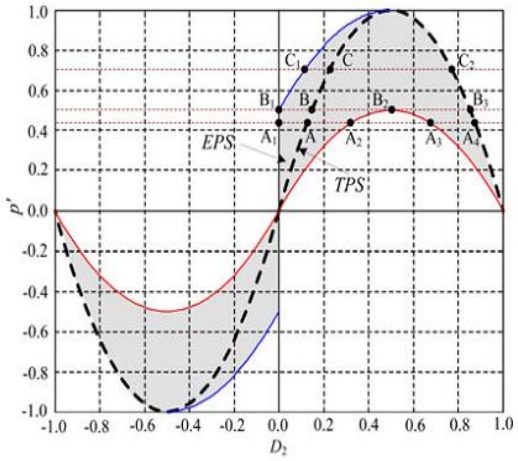

Fig. 3.2. Relation curves of the unified transmission power p' with D_1 and D_2. (2-D curves.)

When taking that the outer phase-shift ratio (D_2) in EPS control is equal to the phase-shift ratio (D) in TPS control, the 3-Dcurves of the unified transmission power p and p varied with D_1 andD_2 shown in Fig. 8(a).As can be

seen from Fig. 3.1, with different D_1 , p' will be different with p. And the EPS control can achieve larger transmission power than the TPS does when $0 \le D_2 < 0.5$. In fact, from Eqn. (3.13), we can derive

$$p'_{max} = 1 - \frac{(1-2D_2)^2}{2} \quad \text{... (3.15)}$$

Where $0 \le D_2 < 0.5$ and $D_1 = 1 - \frac{1-2D_2}{2}$

$$p'_{max} = 4D_2(1 - D_2) \quad \text{... (3.16)}$$

Where $0.5 \le D_2 < 1$ and $D_1 = 0$

$$p'_{min} = 2D_2(1 - D_2) \quad \text{... (3.17)}$$

Where $D_1 = 1 - D_2$

From Eqn. (3.15) to Eqn. (3.17), Fig. 3.1 can be converted to a 2-D picture, as shown in Fig. 3.2. The dashed line is the regulating curve of transmission power in TPS control, and the dark-shaded area is the regulating area of transmission power in EPS control. From Fig. 3.2, due to the addition of D_1, the regulating range of transmission power is changed from the single curve to the 2-D area. With the same outer phase-shift ratio (D_2 = D), the EPS control offers wider power transmission range than the TPS control does, and the maximum value is determined by Eqn. (3.15) and Eqn. (3.16) while the minimum value is determined by Eqn. (3.17). Due to the addition of D_1 , the regulating flexibility of transmission power is also enhanced.

Considering that the basic prerequisite for comparative analysis of backflow power and current stress is that the transmission power of TPS and EPS control are the same. In the following analysis, we take operating points A/A_4 , B/B_3 , and C/C_2 as characteristic points of TPS control in different operating areas, where A(D = 1/8), A_4 (D = 7/8), B(D = (2 – 2^1/2)/4), B3 (D = (2+2^1/2)/4), C(D = 1/4), and C_2 (D = 3/4), then the characteristic points of EPS control are A_1 /A_2 /A_3 , B_1 /B_2 , and C_1.

3.3 Comparative Analysis of Backflow Power

Considering the relationship between the backflow power and the transmission power, the unified backflow power M_{bf} and M'_{bf} are defined as

$$M'_{bf} = \frac{P'_{bf}}{P_N} = \frac{[k(1-D_1)+(2D_2-1)]^2}{2(k+1)} \quad \text{... (3.18)}$$

$$M_{bf} = \frac{P'_{bf}}{P_N} = \frac{[k+(2D-1)]^2}{2(k+1)} \quad \text{... (3.19)}$$

The basic prerequisite for comparative analysis of backflow power is that the transmission power of TPS and EPS control are the same. From Eqn. (3.5) and Eqn. (3.9), we have

$$4D(1 - D) = 4D_2(1 - D_2) + 2D_1(1 - D_1 - 2D_2) \quad \text{... (3.20)}$$

With the specified value of D1 and D2 in EPS control, the phase-shift ratio D in TPS control can be obtained

$$D = \begin{cases} D' = \frac{1-\sqrt{1-4D_2(1-D_2)-2D_1(1-D_1-2D_2}}{2} \\ D'' = \frac{1+\sqrt{1-4D_2(1-D_2)-2D_1(1-D_1-2D_2}}{2} \end{cases} \quad \text{... (3.21)}$$

Using Eqn. (3.18), Eqn. (3.19), and Eqn. (3.20), and assuming k = 5, the 3-D curve of the unified backflow power varied with D_1 and D_2 can be shown in Fig. 3.3. As can be seen from Fig. 3.3, the backflow power in TPS and EPS control are the same when D_1 = 0. And due to the addition of D_1 , with the same transmission power, the backflow power in TPS control is larger than that in EPS control, and the condition of D = D″ generates larger backflow power than the condition of D = D′ does.

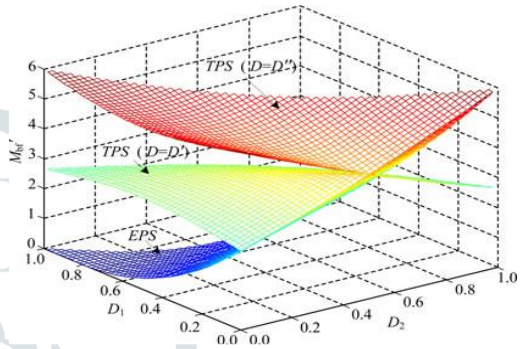

Fig. 3.3. 3-D curves of the unified backflow power M'_{bf} varied with D1 and D2.

The contour lines in Fig. 3.2 show that there are infinite combinations of (D_1, D_2) in EPS control for the same transmission power in TPS control. Considering the different qualities of EPS control in different operating points, we will analyze the optimal operating point of backflow power. From Eqn. (3.20), we have

$$D_1 = \begin{cases} D'_1 = \frac{1-2D_2-\sqrt{2(1-2D)^2-(1-2D_2)^2}}{2} \\ D''_1 = \frac{1-2D_2+\sqrt{2(1-2D)^2-(1-2D_2)^2}}{2} \end{cases} \quad \text{..(3.22)}$$

For $D''_1 \ge D'_1$, from (Eqn. (4.18),we have

$$M''_{bf}(D'_1) \ge M'_{bf}(D''_1) \quad \text{... (3.23)}$$

Substituting $D_1 = D''_1$ into (24), the function of M'_{bf} and D_2 can be obtained

$$M'_{bf\,min}(D_2) = \frac{[k(1-\sqrt{2(1-2D)^2-(1-2D_2)^2})+2(k+2)D_2-2]^2}{8(k+1)} \quad \text{... (3.24)}$$

Where $|1–2D_2| \le 2^1/2\ |1–2D|$ and $0 \le D_2 \le 1$. Solving Eqn. (3.24) with constrained optimization methods, we can derive

1) when $0 \le D < (2–2^1/2)/4$

$$M'_{bf\,min}(D_2) = M'_{bf\,min}(0) = [k - 2 - k\sqrt{2(1-2D)^2-1}]^2 \quad \text{... (3.25)}$$

Where

$$\begin{cases} D_1 = \frac{1+\sqrt{2(1-2D)^2-1}}{2} \\ D_2 = 0 \end{cases}$$

... (3.26)

2) when $(2-2^1/2)/4 \le D < ½$

$$M'_{bf\ min}(D_2) = M'_{bf\ min}\left(\frac{1-\sqrt{2}(1-2D)}{2}\right) = \frac{[(\sqrt{2}-1)-2(k+2)D]^2}{4(k+1)}$$

... (3.27)

Where

$$\begin{cases} D_1 = \frac{\sqrt{2}(1-2D)}{2} \\ D_2 = \frac{1-\sqrt{2}(1-2D)}{2} \end{cases}$$

... (3.28)

In Fig. 3.2, we take operating points *A*, *B*, *C*, A_1 /A_2 /A_3 ,B_1 /B_2 , and C_1 as characteristic points of TPS and EPS control in differ- ent operating areas, from (3.19) to (3.21), and (3.26), we have: A_1 (D_2 = 0, D_1 = (4+2^1/2)/8), A_1 (D_2 = 0, D_1 = (4–2^1 /2)/8), A_2 (D_2 = (4–2^1/2)/8, D_1 = (4+2^1/2)/8), A_3 (D_2 = (4+2^1/2)/8, D_1 = (4–2^1/2)/8), B_1 (D_2 =0,D_1 =1/2), B_2 (D_2 =1/2,D_1 =1/2), and C_1 (D_2 = (2–2^1/2)/4, D_1 = 2^1/2/4). Fig. 3.4,3.5,3.6 shows the curves of the unified backflow power varied with voltage conversion ratio k in TPS and EPS control for the same transmission power.

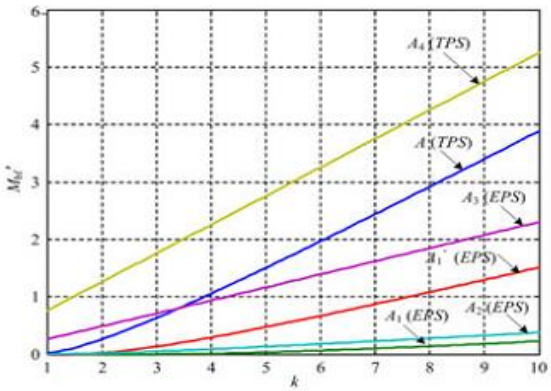

Fig.3.4 Curves of the unified backflow power M'_{bf} varied with voltage conversion ratio k (*A* and A_4 in TPS control and A_1 , A'_1 , A_2 ,and A_3 in EPS control.)

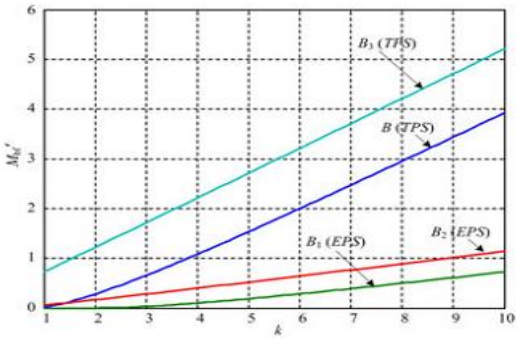

Fig.3.5 Curves of the unified backflow power M'_{bf} varied with voltage conversion ratio k (*B* and B_3 in TPS control and B_1, B_2 in EPS control.)

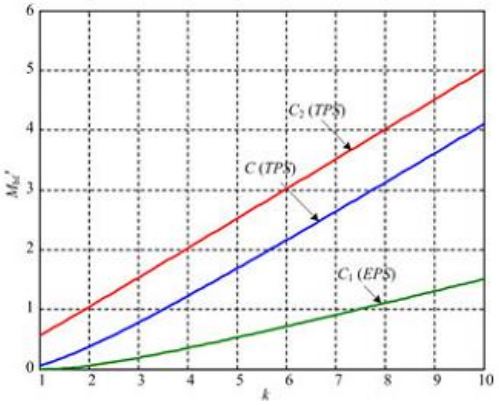

Fig.3.6 Curves of the unified backflow power M'_{bf} varied with voltage conversion ratio k (*C* and C_2 in TPS control and C_1 in EPS control.)

3.4 Comparative Analysis of Current Stress

For the convenience of analysis, the unified current stress *G* and *G* are defined as

$$G' = \frac{i'_{max}}{I_N} = 2[k(1-D_1) + (2D_1 + 2D_2 - 1)]$$ ... (3.29)

$$G = \frac{i'_{max}}{I_N} = 2(2D - 1 + k)$$ ... (3.30)

Where

$$I_N = \frac{P_N}{V_1} = \frac{nV_2}{8f_sL}$$ ... (3.31)

Using Eqn. (3.21), Eqn. (3.29), and Eqn. (3.30), and assuming k = 5, the 3-D curve of the unified current stress varied with D_1 and D_2 as shown in Fig. 3.3. As can be seen from Fig. 3.3, the current stress in TPS and EPS control are the same when D_1 = 0. And due to the addition of D_1 with the same transmission power, the current stress in TPS control is larger than that in EPS control, and the condition of $D = D''$ generates larger current stress than the condition of $D = D'$ does.

Likewise, the optimal operating point of current stress can be analyzed. For $D''_1 \ge D'_1$, from Eqn. (3.29), we have

$$\begin{cases} G'(D'_1) \le G(D''_1) & k < 2 \\ G'(D''_1) \le G(D'_1) & k \ge 2 \end{cases}$$ ... (3.32)

That is,

$$G'_{min} = \begin{cases} (k-2)\sqrt{2(1-2D)^2 - (1-2D_2)^2} + 2kD_2 + k & k < 2 \\ (2-k)\sqrt{2(1-2D)^2 - (1-2D_2)^2} + 2kD_2 + k & k \ge 2 \end{cases}$$ ... (3.33)

1) Where $|1-2D_2| \le 2^1/2\ |1-2D|$ and $0 \le D_2 \le 1$. Solving Eqn. (3.33) with constrained optimization methods, we can derive

$$G'_{min}(D_2) = \begin{cases} (k-2)\sqrt{2(1-2D)^2 - 1} + k & k < 2 \\ (2-k)\sqrt{2(1-2D)^2 - 1} + k & k \ge 2 \end{cases}$$ ... (3.34)

Where

$$\begin{cases} D_1 = \begin{cases} \frac{1-\sqrt{2(1-2D)^2-1}}{2} & k < 2 \\ \frac{1+\sqrt{2(1-2D)^2-1}}{2} & k \geq 2 \end{cases} \\ D_2 = 0 \end{cases} \quad \text{... (3.35)}$$

According to Eqn. (3.28) and Eqn. (3.35), when k≥2, the optimal operating points of backflow power and current stress are the same. From Eqn. (3.30) and Eqn. (3.34), we can derive

$$\begin{cases} G \leq G'_{min} & k < k_0 \\ G'_{min} \leq G & k \geq k_0 \end{cases} \quad \text{... (3.36)}$$

$$k_0 = 2 - \frac{1+\sqrt{2(1-2D)^2-1}}{2(1-D)} \quad \text{... (3.37)}$$

2) when $(2-2^1/2)/4 \leq D < ½$

$$G'_{min}(D_2) = k(2\sqrt{2}D + 2 - \sqrt{2} \quad \text{... (3.38)}$$

Where

$$\begin{cases} D_1 = \frac{\sqrt{2}(1-2D)}{2} \\ D_2 = \frac{1-\sqrt{2}(1-2D)}{2} \end{cases} \quad \text{...(3.39)}$$

From Eqn. (3.30) and Eqn. (3.38), we can derive

$$\begin{cases} G \leq G'_{min} & k < k_0 \\ G'_{min} \leq & k \geq k_0 \end{cases} \quad \text{... (3.40)}$$

Wher

$$k_0 = \sqrt{2} \quad \text{.. (3.41)}$$

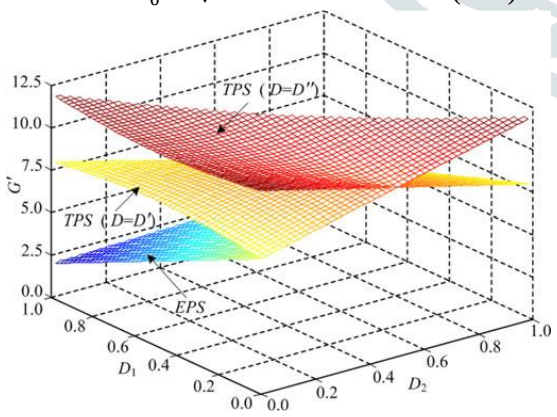

Fig. 3.7. 3-D curves of the unified current stress *G* varied with D_1 and D_2.

According to the above analysis, when $k \geq k_0$, the current stress in EPS control is less than that in TPS control. Likewise, we take operating points *A*, *B*, *C*, A_1 /A_2 /A_3, B_1 /B_2 , and C_1 as characteristic points of TPS and EPS control in different operating areas. Then the curves of the unified current stress varied with voltage conversion ratio k for the same transmission power shown in Fig. 3.8,3.9,3.10.

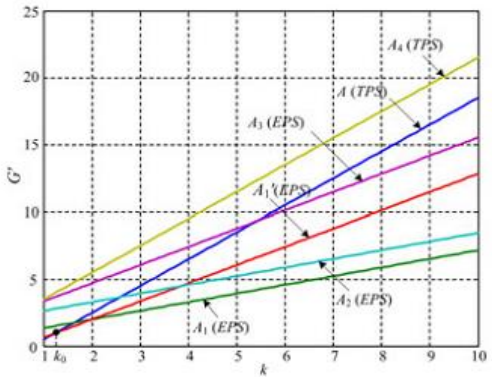

Fig.3.8 Curves of the unified current stress *G* varied with voltage conversion ratio k (*A* and A_4 in TPS control and A_1 , A'_1 , A_2 ,and A_3 in EPS control.)

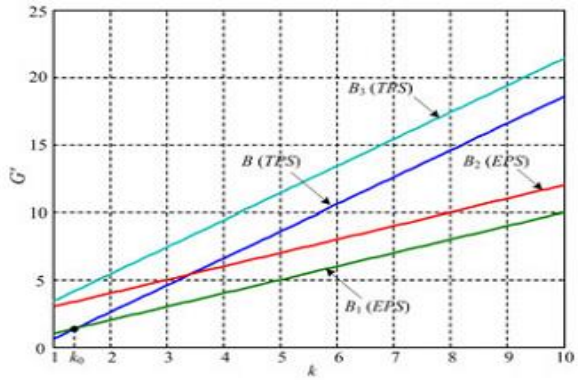

Fig.3.9 Curves of the unified current stress *G* varied with voltage conversion ratio k (*B* and B_3 in TPS control and B_1, B_2 in EPS control.)

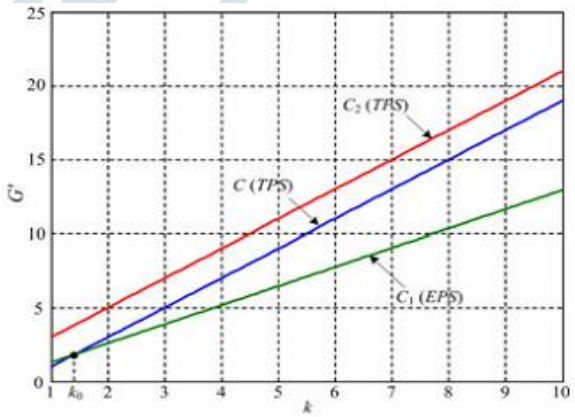

Fig.3.10 Curves of the unified current stress *G* varied with voltage conversion ratio k ratio k (*C* and C_2 in TPS control and C_1 in EPS control.)

As can be seen from Fig. 3.8, 3.9, 3.10 in all operating areas, the current stress increases with the increase of voltage conversion ratio k. The EPS control can take different operating points to ensure that the current stress is less than the TPS control when k ≥ k0 , and the minimum value is obtained at A_1,B_1, and C_1 , which agrees well with the aforementioned theoretical analysis.

3.5 Summery

Analysis of above parameters, we can derive that the current stress of converter under EPS control is

$$i'_{max} = \frac{V_1}{4f_sL}\left[\frac{1}{k}(1-D_1)+(2D_1+2D_2-1)\right]$$

... (3.42)

The transmission power is

$$P' = \frac{nV_1V_2}{2f_sL}\left[D_2(1-D_1)+\frac{1}{2}D_1(1-D_1-2D_2)\right]$$

... (3.43)

The backflow power is

$$P'_{bf} = \frac{nV_1V_2[(1/k)(1-D_1)+(2D_2-1)]^2}{16f_sL(1/k+1)}$$ ... (3.44)

In Eqn. (3.42) – Eqn. (3.44), the constraints are $k < 1$, $0 \le D_1 \le 1$, $0 \le D_2 \le 1$ and $0 \le D_1+D_2 \le 1$. Similarly, the current stress of converter under TPS control is

$$i_{max} = \frac{V_1}{4f_sL}(2D-1+1/k)$$ ... (3.45)

The transmission power is

$$P = \frac{nV_1V_2}{2f_sL}D(1-D)$$ ... (3.46)

The backflow power is

$$P_{bf} = \frac{nV_1V_2[(1/k)+(2D-1)]^2}{16f_sL(1/k+1)}$$ ... (3.47)

In Eqn. (3.45) – Eqn. (3.47), the constraints are $k < 1$ and $0 \le D \le 1$. Due to $1/k > 1$, comparing Eqn. (3.42) – Eqn. (3.47) with Eqn. (3.3) – Eqn. (3.6) and Eqn. (3.8) – Eqn. (3.16), we can come to the conclusion that the performance at $k < 1$is coincident with that at $k > 1$.

Finally, in this chapter we observed the entire analysis of Traditional Phase Shift Control and Extended Phase Shift Control in various parameters like optimal power flow, back power flow, and current stress. In the next chapter we shall observe the outputs of above analysis.

4. SIMULATION RESULTS

Table 4.1 Comparative analysis of TPS and EPS controls in IBDC

S.NO	PARAMETER	TPS	EPS
1	Design of Control Scheme	Easy	Complex
2	Level of control scheme	Two	Three
3	Back flow Power	High	Low
4	Regulating range of Transmission Power	High	Low
5	Regulating Flexibility	High	Low
6	Circulating Power Flow	High	Low
7	Current Stress	High	Low
8	Switching Loss	High	Low
9	Life of Devices	High	Low
10	Conduction Loss	High	Low
11	System Efficiency	High	Low

5. CONCLUSIONS

5. Conclusion

Isolated Bi-Directional DC-DC Converter (IBDC) is an everlasting key component to realize power distribution in between energy generation systems and energy storage systems in microgrids. In order to overcome the inherent disadvantages of Traditional Phase Shift (TPS) control of Isolated Bi-Directional DC-DC Converter like great circulating power, great circulating currents, loss in power devices and magnetic components and low efficiency, a novel Extended Phase Shift control is proposed for power distribution in microgrid in this project. From the theoretical analysis it can be found that Extended Phase Shift control has the following features:

1) EPS control expands regulating range of transmission power and enhances regulating flexibility.

2) EPS control reduces power-circulating flow, and thus reduces conduction losses and improves the system efficiency.

3) EPS control reduces current stress, and thus reduces switching losses and prolongs the service life of devices. For the same power level, the devices can be selected with lower stress levels, which saves the cost.

4) EPS control is simple in principle and easy to implement.

Then the following table will give the comparative analysis of the two methods i.e the Traditional Phase Shift control and The Extended Phase Shift control technique in Isolated Bi-Directional DC-DC Converter in the various parameters like backflow power, regulating range of transmission power, regulating flexibility, power circulating flow, current stress, switching loss, life of devices, conduction loss and system efficiency.

REFERENCES

[1] Biao Zhao, Student Member, IEEE, Qingguang Yu, Member, IEEE, and Weixin Sun, "Extended-Phase-Shift Control of Isolated Bidirectional DC–DC Converter for Power Distribution in Microgrid" IEEE Transactions On Power Electronics, Vol. 27, No. 11, November 2012

[2] R. H. Lasseter, "Smart distribution: Coupled microgrids," Proc. IEEE., vol. 99, no. 6, pp. 1074–1082, Jun. 2011.

[3] P. Tenti, H. K. M. Paredes, and P. Mattavelli, "Conservative power theory, a framework to approach control and accountability issues in smart microgrids," IEEE Trans. Power Electron., vol. 26, no. 3, pp. 664–673, Mar. 2011.

[4] R. Majumder, A. Ghosh, G. Ledwich, and F. Zare, "Power management and power flow control with back-to-back converters in a utility connected microgrid," IEEE Trans. Power System., vol. 25, no. 2, pp. 821–834,May 2010.

[5] A. K. Abdelsalam, A. M. Massoud, S. Ahmed, and P. N. Enjeti, "High-performance adaptive perturb and observe MPPT technique for photovoltaic-based microgrids," IEEE Trans. Power Electron., vol. 26, no. 4, pp. 1010–1021, Apr. 2011.

[6] J. M. Guerrero, J. C. Vasquez, J. Matas, M. Castilla, and L. G. Vicuna, "Control strategy for flexible microgrid based on parallel line-interactive UPS system," IEEE Trans. Ind. Electron., vol. 56, no. 3, pp. 726–736, Mar. 2009.

[7] J. Y. Kim, J. H. Jeon, S. K. Kim, C. Cho, J. H. Park, H.-M. Kim, and K.-Y. Nam, "Cooperative control strategy of energy storage system and microsources for stabilizing the microgrid during islanded operation," IEEE Trans. Power Electron., vol. 25, no. 12, pp. 3037–3048, Dec. 2010.

[8] J.-H. Jeon, J.Y.Kim,H.M.Kim, S.-K.Kim, C. Cho, J.-M.Kim, J.-B.Ahn, and K.-Y. Nam, "Development of hardware in-the-loop simulation system for testing operation and control functions of microgrid," IEEE Trans. Power Electron., vol. 25, no. 12, pp. 2919–2929, Dec. 2010.

[9] T. F. Wu, K. H. Sun, C. L. Kuo, and C. H. Chang, "Predictive currentcontrolled 5-kW single-phase bidirectional inverter with wide inductance variation for dc-microgrid applications," IEEE Trans. Power Electron., vol. 25, no. 12, pp. 3076–3084, Dec. 2010.

[10] M. G. Molina and P. E. Mercado, "Power flow stabilization and control of microgrid with wind generation by superconducting magnetic energy4680 storage," IEEE Trans. Power Electron., vol. 26, no. 3, pp. 910–922, Mar. 2011.

[11] J.M. Gueerrero, N. Berbel, J.Matas, J. L. Sosa, and L. G. vicuna, "Droopcontrol method with virtual output impedance for parallel operation of uninterruptible power supply systems in a microgrid," in Proc. IEEE Appl. Power Electron. Conf., 2007, pp. 1126–1132.

[12] W. Chen, P. Rong, and Z. Y. Lu, "Snubberless bidirectional DC–DC converter with new CLLC resonant tank featuring minimized switching loss," IEEE Trans. Ind. Electron., vol. 57, no. 9, pp. 3075–3086, Sep. 2010.

[13] F. H. Khan and L. M. Tolbert, "Bi-directional power management and fault tolerant feature in a 5-kWmultilevel DC–DC converter with modular architecture," IET Power Electron., vol. 2, no. 5, pp. 595–604, Jul. 2009.

[14] C.M.Wang, C. H. Lin, and T. C. Yang, "High-power-factor soft-switched DC power supply system," IEEE Trans. Power Electron., vol. 26, no. 2, pp. 647–654, Feb. 2011.

[15] P. Das, S. A. Mousavi, and G. Moschopoulos, "Analysis and design of a nonisolated bidirectional ZVS-PWM DC–DC converter with coupled inductors," IEEE Trans. Power Electron., vol. 25, no. 10, pp. 2630–2641, Oct. 2010.

[16] K. R. Wang, F. C. Lee, and J. Lai, "Operation principles of bi-directional full-bridge DC-DC converter with unified soft-switching scheme and soft starting capability," in Proc. IEEE Appl. Power Electron. Conf., 2000, pp. 111–118.

[17] B. Hua and M. Chris, "Eliminate reactive power and increase system efficiency of isolated bidirectional dual-active-bridge DC–DC convert-ers using novel dual-phase-shift control," IEEE Trans. Power Electron., vol. 23, no. 6, pp. 2905–2914, Nov. 2008.

[18] H. Fan and H. Li, "A novel phase-shift bidirectional DC–DC converter with an extended high-efficiency range for 20kVAsolid state transformer," in Proc. IEEE Energy Convers. Congr. Expo. (ECCE)., 2010, pp. 3870 3876.

[19] S. Inoue and H. Akagi, "A bidirectional DC–DC converter for an energy storage system with galvanic isolation," IEEE Trans. Power Electron., vol. 22, no. 6, pp. 2299–2306, Nov. 2007.